

Optimizing current harmonics compensation in three-phase power systems with an Enhanced Bacterial foraging approach



Sushree Sangita Patnaik*, Anup Kumar Panda

Department of Electrical Engineering, National Institute of Technology, Rourkela, India

ARTICLE INFO

Article history:

Received 17 April 2013

Received in revised form 21 March 2014

Accepted 24 March 2014

Keywords:

Active power filter

Current harmonics

Real-time analysis

Bacterial foraging optimization

Particle swarm optimization

ABSTRACT

A shunt active power filter (APF) comprising of pulse-width modulation (PWM) based voltage-source inverter (VSI) is presented in this paper, because it has grabbed tremendous attention as a promising power conditioner. However, it involves huge power loss due to the presence of inductors and semiconductor switching devices, resulting in deterioration of APF performance. So, a Proportional–Integral (PI) controller has been used to minimize this undesirable power loss by regulating the dc-link voltage of VSI. Conventional linearized tuning of PI controller gains does not yield satisfactory results for a range of operating conditions due to the complex, non-linear and time-varying nature of power system networks. The goal of this paper is to find out optimized values of PI controller gains by the implementation of optimization techniques. Developed by hybridization of Particle swarm optimization (PSO) and Bacterial foraging optimization (BFO), an Enhanced BFO technique is presented in this paper so as to overcome the drawbacks in both PSO and BFO, and accelerate the convergence of optimization problem. Comparative evaluation of PSO, BFO and Enhanced BFO has been carried out with regard to compensation of harmonics in source current in a three-phase three-wire system. Extensive MATLAB simulations followed by real-time performance analysis in Opal-RT Lab simulator validate that, the APF employing Enhanced BFO gives superior load compensation compared to the other alternatives, under a range of supply and sudden load change conditions. It drastically lowers down the source current total harmonic distortion (THD), thereby satisfying the IEEE-519 standard recommendations on harmonic limits.

© 2014 Elsevier Ltd. All rights reserved.

Introduction

Current harmonics resulted due to the increased usage of non-linear loads, are the major culprits behind poor efficiency and power factor, increased losses in power system, electro-magnetic interference (EMI) with nearby communication lines, false tripping of protective relays, failure or misoperation of microprocessors, vibration in rotating machines, voltage quality degradation, malfunctioning of medical facilities, and overheating of transformers, motors, neutral conductors, etc. [1,2]. IEEE Recommended Practices and Requirements for Harmonic Control in Electric Power Systems (IEEE 519-1992 Standard) [3,4] do an excellent job providing a basis for limiting harmonics. The shunt APF is devised to suppress different orders of harmonics simultaneously by injecting current harmonics of equal magnitude but in phase opposition with the load current harmonics at the point of common coupling (PCC) between the source and the load as shown in Fig. 1, thereby canceling out each other [5–8]. This can overcome the shortcomings of

traditional passive filters like fixed compensation, large size, increased risk of harmonic resonance with power system impedance, and ineffectiveness when the harmonic content in load current varies randomly [8,9]. Compensation currents generated by the shunt APF can simultaneously compensate for current harmonics and reactive power (also neutral current and unbalanced loading of utility in three-phase four-wire systems) [6,10]. Various control schemes have been proposed since the development of APFs [11–13]. But with i_d-i_q method, harmonics can be mitigated under all kinds of supply voltages [14,15].

During steady state operation, real power supplied by the source is equal to the real power demand of loads plus a small power to compensate the switching and conduction losses of Insulated gate bipolar transistors (IGBTs) inside APF. However during load variation, real power difference between the two is compensated by the charging/discharging of dc-link capacitor of VSI. For proper functioning of APF, dc-link voltage should be maintained constant with the help of a PI controller [16]. APFs with conventional PI controller yield inadequate results under a range of operating conditions [17,18], and are also criticized for being case dependent because, when they are applied to same model with

* Corresponding author.

E-mail address: sspatnaik.ee@gmail.com (S.S. Patnaik).

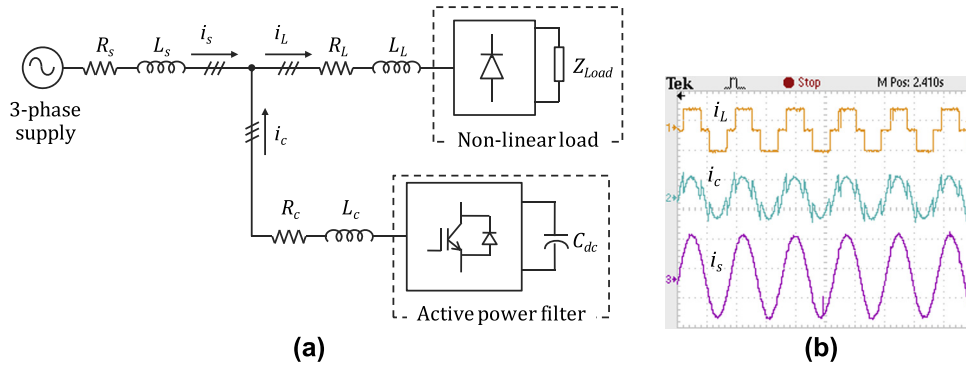


Fig. 1. Compensation principle of shunt APF (a) schematic diagram and (b) waveforms for load current (i_L), filter current (i_c) and compensated source current (i_s).

different parameters, the result varies. Hence load compensation capability of APF can be enhanced by optimizing the gains of PI controller [19–21]. Few solutions to the harmonic mitigation problem are found in Refs. [22,23], where harmonics are minimized through an objective function by optimization. In recent years, many advances have been made to solve optimization problems in various fields of application and research by the use of Simulated annealing, Tabu search, Genetic algorithm (GA), Ant colony optimization (ACO), Artificial Bee colony (ABC) optimization, PSO, BFO, etc. Some artificial-intelligence based techniques such as Fuzzy logic, Neural network and GA are exploited in Ref. [24] to design a control scheme for APFs dealing with harmonic and reactive current compensation.

PSO was introduced by Kennedy and Eberhart, and is being extensively used due to its simple concept, easy implementation, inexpensive computation and well-balanced mechanism to promote both local and global explorations [15,19,20,25–27]. Na He et al. demonstrated PSO to be effective and suitable for multi-objective optimal design of filters [28]. In spite of so many advantages, it suffers from the severe drawback of premature convergence [29,30]. Since the inception in 2002, BFO has drawn the attention of researchers to solve real-world problems such as adaptive control [31], harmonic signal estimation [32], optimal power system stabilizers design [33,34], and optimization of real power loss and voltage stability limit [35]. It is also hybridized with few other state-of-the-art evolutionary computation techniques [36–39] in order to achieve robust and efficient search performances. Over certain real-world optimization problems, BFO is reported to outperform many powerful optimization algorithms like GA and PSO in terms of convergence speed and final accuracy [18,31,32,35,37,38]. An approach based on BFO was proposed by Mishra that validated optimal control of APF under sudden switch-on, load change and filter parameters variation with ideal supply voltage [17]. However, there is no explanation towards the performance of APF when there is a huge unbalance or distortion in supply voltage along with sudden load variation. In our previous work [18], a comparative evaluation of conventional, PSO and BFO based APFs was carried out under ideal and unbalanced supply without any load variation. Here the performance is investigated under ideal, distorted and unbalanced supplies with sudden load variation in MATLAB followed by real-time performance analysis in Opal-RT Lab. BFO has also been reported to suffer from problems due to its fixed step size and uncontrolled particle velocities [34,40–42]. Step size of the bacteria is decided by their velocities. Large step size leads to lesser accuracy though the particles arrive at vicinity of optima quickly; whereas smaller step size slows down the convergence process.

A more powerful search algorithm called as Enhanced BFO is developed here, with the combined advantages of PSO and BFO. This is found to be faster and provide more accurate results

compared to the usual PSO and BFO. Results obtained with MATLAB/Simulink simulations are compared for APF employing PSO, BFO and Enhanced BFO. It revealed that, Enhanced BFO shows quick convergence to reach the desired solution thereby yielding superior solution quality. Now-a-days, the testing and validation of power conditioning devices is very essential in the design and engineering process. The need for constant improvement of component modeling has led to an increase in the speed of system prototyping. But this has two major drawbacks. (i) There is a big hurdle in the design process during the leap over from off-line simulation to real prototype, as it is prone to many troubles related to the integration of different modules at a time. (ii) Off-line non-real-time simulation becomes tediously long for any moderately complex system. With advance in real-time simulation techniques, RT-Lab simulator developed by Opal-RT technologies emerged as a promising tool. It is an industrial grade, scalable and real-time platform for simulation, control testing and related applications [15,43,44]. Though several papers based on the implementation of evolutionary algorithms are there in literature, this paper describes their performances and figures out the efficiency of these algorithms in real-time using Opal-RT Lab simulator.

Shunt active power filter

Several aspects to be considered while designing an APF are topology, reference compensation current extraction scheme and PWM technique used to produce switching signals. Shunt APFs are generally developed with either of the two types of PWM converters; current-source inverter (CSI) or voltage-source inverter (VSI) [6,45,46]. However, the latter is preferred as it is lighter, cheaper, and expandable to multilevel and multistep versions for improved performance in high power ratings with lower switching frequencies [6,46]. Fig. 2 depicts the system configuration of shunt APF with non-linear load.

In Fig. 3, the block diagram for reference current generation employing i_d-i_q control scheme has been illustrated. The load currents i_{La} , i_{Lb} and i_{Lc} are tracked, upon which Park's transformation is performed to obtain corresponding $d-q$ axes currents i_{Ld} and i_{Lq} as given in (1), where ω is the rotational speed of synchronously rotating $d-q$ frame.

$$\begin{bmatrix} i_{Ld} \\ i_{Lq} \end{bmatrix} = \begin{bmatrix} i_{Ld1h} + i_{Ldnh} \\ i_{Lq1h} + i_{Lqnh} \end{bmatrix} = \frac{\sqrt{2}}{3} \begin{bmatrix} \cos \omega t & \sin \omega t \\ -\sin \omega t & \cos \omega t \end{bmatrix} \begin{bmatrix} 1 & -\frac{1}{2} & -\frac{1}{2} \\ 0 & \frac{\sqrt{3}}{2} & -\frac{\sqrt{3}}{2} \end{bmatrix} \begin{bmatrix} i_{La} \\ i_{Lb} \\ i_{Lc} \end{bmatrix} \quad (1)$$

According to i_d-i_q control strategy, only the average value of d -axis component of load current should be drawn from supply. Here i_{Ld1h} and i_{Lq1h} indicate the fundamental frequency components of i_{Ld} and i_{Lq} respectively. The oscillating components i_{Ld} and i_{Lq} , i.e.,

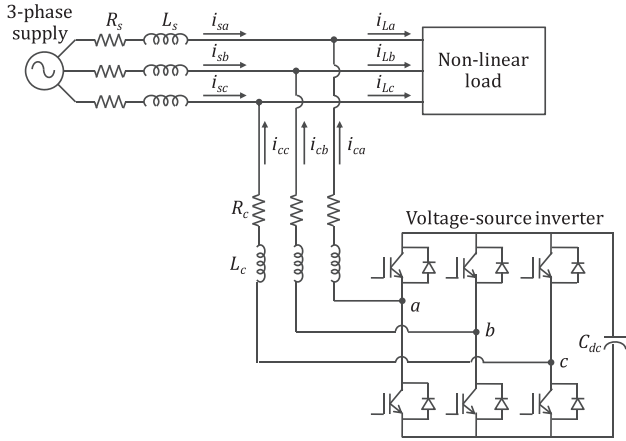


Fig. 2. Configuration of shunt APF with non-linear load.

i_{Ldnh} and i_{Lqnh} are filtered out using low-pass filter (LPF) consisting of 2nd order Butterworth type filters with cut-off frequency of 25 Hz. Signal i_{d1h} accounts for the losses occurring in VSI and can be obtained from dc-link voltage regulator explained in Section ‘Problem formulation’. Currents i_{Ldnh} and i_{Lqnh} along with i_{d1h} are utilized to generate reference filter currents i_{cd}^* and i_{cq}^* in $d-q$ coordinates, followed by inverse Park’s transformation giving away the compensation currents i_{ca}^* , i_{cb}^* and i_{cc}^* in the three wires as described in (2).

$$\begin{bmatrix} i_{ca}^* \\ i_{cb}^* \\ i_{cc}^* \end{bmatrix} = \begin{bmatrix} \sin \omega t & \cos \omega t & 1 \\ \sin (\omega t - \frac{2\pi}{3}) & \cos (\omega t - \frac{2\pi}{3}) & 1 \\ \sin (\omega t + \frac{2\pi}{3}) & \cos (\omega t + \frac{2\pi}{3}) & 1 \end{bmatrix} \begin{bmatrix} i_{cd}^* \\ i_{cq}^* \\ i_{c0}^* \end{bmatrix} \quad (2)$$

The zero-sequence reference current i_{c0}^* in (2) is used just to make the transformation matrix a square one. The continuously tracked actual filter currents (i_{ca} , i_{cb} , i_{cc}) are compared with the reference filter currents (i_{ca}^* , i_{cb}^* , i_{cc}^*) in a Hysteresis band current controller and consequently switching signals are generated [15]. Hysteresis PWM is used here for instantaneous harmonic compensation by the APF on account of simple implementation and quick prevail over fast current transitions. The main drawback of Hysteresis current control is its high switching frequency that results in generation of some higher order harmonics due to the frequent switching of semiconductor devices, which can be eliminated using RC high-pass filter. Power losses that take place inside VSI as a consequence of this high frequency switching are minimized by dc-link voltage regulator.

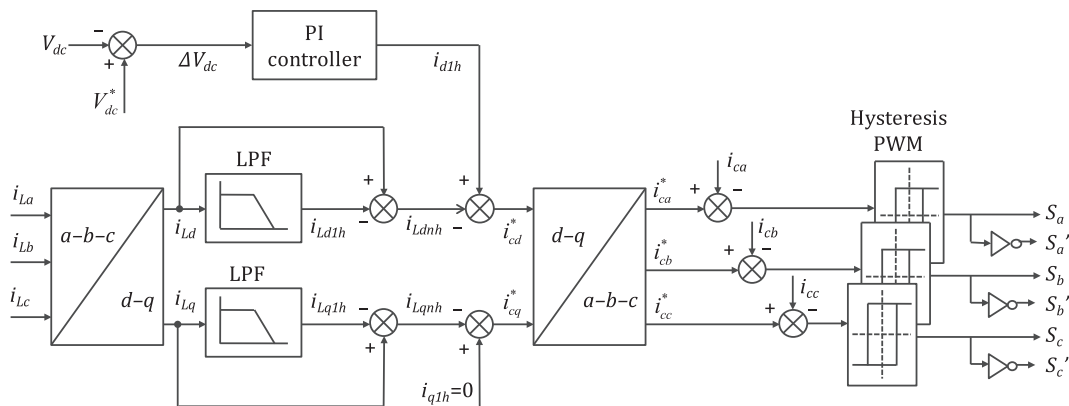


Fig. 3. Reference compensation current extraction and generation of switching signals.

Optimization approaches

Particle swarm optimization

Inspired by the social behavior of organisms in a bird flock or fish school, this optimization technique emerged as a promising nature-inspired stochastic approach of evolutionary computation in the year 1995. Each candidate solution is a parameter vector called as particle. The mechanism of PSO is initialized with a group of randomly dispersed particles assigned with some arbitrary velocities. The particles fly through the problem space in search of global optimum position. The PSO system combines a social-only model and a cognition-only model [26,47]. The social-only component suggests the individuals to ignore their own experiences and adjust their behavior according to the intelligence of neighboring individuals. In contrast, cognition-only component treats the individual experience of each particle.

The particles update their positions and velocities in accordance with (3) and (4), formulated by taking into consideration both the social-only and cognition-only components.

$$v_{k+1}^i = w \cdot v_k^i + c_1 \cdot r_1 \cdot [x_{Lbest}^i - x_k^i] + c_2 \cdot r_2 \cdot [x_{Gbest}^i - x_k^i] \quad (3)$$

$$x_{k+1}^i = x_k^i + v_{k+1}^i \quad (4)$$

In the above expressions,

k and i are indices for number of iterations and particle number; x_k^i and v_k^i are current position and velocity of i th particle at k th iteration;

x_{k+1}^i and v_{k+1}^i are position and velocity of i th particle at $(k + 1)$ th iteration;

w , c_1 and c_2 are inertia, cognitive and social constants; r_1 and r_2 are random numbers in the interval $[-1, 1]$.

Acceleration of particles is decided by the values of constants c_1 and c_2 , whereas w provides a sense of balance between local and global search. The exploration of new search space depends upon the value of w . Eberhart and Shi proposed a value of w that decreases linearly with successive iterations [48], given as:

$$w = w_{max} - (w_{max} - w_{min}) \frac{g}{G} \quad (5)$$

where g is the index representing the current number of evolutionary generation, G is the predefined maximum number of generations, and w_{max} and w_{min} are maximal and minimal inertial weights. Initially, the value of w is taken 0.9 (maximum) in order to allow the particles to find the global optimum neighborhood faster. Value of w is set to 0.4 (minimum) upon finding out the optima so that the search is shifted from exploratory mode to exploitative

mode. The search terminates when either the predefined maximum number of iterations are executed or a further better optimum solution is not available.

Bacterial foraging optimization

This optimization approach is based on the foraging behavior exhibited by *E. coli* bacteria inside human intestine. Here the bacteria undergo Natural selection and the ones with poor foraging strategies are eliminated, whereas those with good foraging strategies survive. It was introduced by Passino in 2002 and further established by Mishra in the year 2005 for harmonic estimation in power system voltage/current waveforms. BFO mimics four principal mechanisms observed in bacteria viz. chemotaxis, swarming, reproduction and elimination–dispersal.

Chemotaxis

If θ and $J(\theta)$ represent the position and fitness of a bacterium, we want to find the minimum of $J(\theta)$, $\theta \in \mathbb{R}^P$; where we do not have measurements or an analytical description of the gradient $\nabla J(\theta)$. Following are the three conditions that arise

- (i) $J(\theta) < 0$; nutrient-rich environment.
- (ii) $J(\theta) = 0$; neutral environment.
- (iii) $J(\theta) > 0$; noxious environment.

Basically, chemotaxis is the movement of *E. coli* bacteria in search of nutrient-rich location, away from noxious environment. This is accomplished with the help of the locomotory organelles known as Flagella. Chemotactic movement is achieved by either of the following two ways,

- (i) Swimming (in the same direction as the previous step).
- (ii) Tumbling (in an absolutely different direction from the previous one).

Suppose $\theta^i(j, k, l)$ represents the i th bacterium at j th chemotactic, k th reproductive and l th elimination–dispersal step. Then movement of the bacterium may be mathematically represented by (6).

$$\theta^i(j+1, k, l) = \theta^i(j, k, l) + C(i) \frac{\Delta(i)}{\sqrt{\Delta^T(i) \cdot \Delta(i)}} \quad (6)$$

In the expression, $C(i)$ is the size of unit step taken in a random direction and $\Delta(i)$ indicates a vector in the arbitrary direction whose elements lie in $[-1, 1]$.

Swarming

This group behavior is seen in several motile species of bacteria, which helps them to propagate collectively as concentric patterns of swarms with high bacterial density while moving up in the nutrient gradient. The cell-to-cell signaling in bacterial swarm via attractant and repellant ($J_{cc}(\theta(i, j, k, l))$) may be modeled as per (7).

$$\begin{aligned} J_{cc}(\theta(i, j, k, l)) &= \sum_{i=1}^S J_{cc}(\theta, \theta^i(j, k, l)) \\ &= \sum_{i=1}^S \left[-d_{att} \cdot \exp \left(-w_{att} \sum_{m=1}^P (\theta_m - \theta_m^i)^2 \right) \right] \\ &\quad + \sum_{i=1}^S \left[h_{rep} \cdot \exp \left(-w_{rep} \sum_{m=1}^P (\theta_m - \theta_m^i)^2 \right) \right] \end{aligned} \quad (7)$$

Here S indicates the total number of bacteria in the population, P is the number of variables to be optimized, $\theta = [\theta_1, \theta_2, \dots, \theta_P]^T$ is a

point in the P -dimensional search domain that represents the positions of bacteria in the swarm, and θ_m^i is the m th component of the i th bacterium position θ^i . The coefficients d_{att} , w_{att} , h_{rep} and w_{rep} are the measures of quantity and diffusion rate of the attractant signal and the repellant effect magnitude respectively. Now, the resulting objective function $J(\theta(i, j, k, l))$ becomes

$$J(\theta(i, j, k, l)) = J(\theta(i, j, k, l)) + J_{cc}(\theta(i, j, k, l)) \quad (8)$$

Reproduction

The fitness value for i th bacterium after travelling N_c chemotactic steps can be evaluated by following (9).

$$J_{health}^i = \sum_{j=1}^{N_c+1} J^i(j, k, l) \quad (9)$$

Here J_{health}^i represents the health of i th bacterium. The least healthy bacteria constituting half of the bacterial population (S_r) are eventually eliminated, while each healthier bacterium asexually reproduce by splitting into two, which are then placed in the same location. Ultimately, the population remains constant. If S number of bacteria constitute the population, then

$$S_r = \frac{S}{2} \quad (10)$$

Elimination and dispersal

It is possible that the local environment where bacterial population live changes either gradually via consumption of nutrients or suddenly due to some other influence such as significant heat rise. Following this behavior, BFO algorithm makes some bacteria to get eliminated and dispersed with probability P_{ed} after N_{re} number of reproductive events. This is to ensure that the bacteria do not get trapped into local optima instead of global optimum.

Enhanced Bacterial foraging optimization

Taking into consideration all the drawbacks and advantages of PSO and BFO algorithms discussed in Section 'Introduction', an Enhanced BFO algorithm is developed here that has the combined advantages of BFO and PSO, and is also capable of overcoming the limitations in both. The performance of PSO is degraded in problems with multiple optima owing to a phenomenon called premature convergence, where the particles tend to converge and ultimately get trapped in a local best position as the global best remains undiscovered. Enhanced BFO overcomes this drawback through elimination–dispersal of bacteria, thereby ensuring convergence to global optimum. Furthermore, the movement of individuals in traditional BFO algorithm is not defined in any specific direction. Random search directions delay the convergence to global solution. However, unlike BFO, at any particular instant in PSO each particle memorizes its own best solution (local best) as well as the best solution of entire swarm (global best) owing to the memory it possesses. Thereby, velocity and direction of particles are obtained as outcome of their social interactions and memory storage capability. This characteristic of PSO is incorporated in Enhanced BFO that improves search efficiency, global optimum solution accuracy and convergence speed, which are the key attributes of an optimization algorithm. In Enhanced BFO, the chemotaxis, swarming, reproduction, and elimination–dispersal events carried out in BFO realizing cell-to-cell communication, survival of the fittest, elimination of least healthy bacteria in the population, and exploration of new search areas is supplemented with the ability of PSO to exchange social information and possession of adaptable particle velocity. Hence, this algorithm yields relatively more optimized result compared to BFO and PSO

implemented alone. The mechanism of Enhanced BFO and the iterative algorithm realizing this mechanism are presented below in detail. A flowchart of the entire Enhanced BFO technique is depicted in Fig. 4.

Mechanism of Enhanced Bacterial foraging optimization

In the beginning of search process, a group of bacteria are randomly dispersed all throughout the search space. Each bacterium is assigned with an arbitrary particle velocity. Fitness values of the bacteria are calculated by taking into consideration the cell-to-cell swarming effect. For the initial population, the local best and global best positions are figured out in exactly same way as done in PSO. In order to update the positions of individuals, chemotaxis is carried out, which utilizes a velocity factor obtained from the velocity update expression used in PSO. After each chemotactic step, fitness value of each particle is calculated. During the search, reproduction and elimination–dispersal events of BFO are also executed. For reproduction, half of the bacterial population with least health are eliminated, while rest half of the population asexually reproduce by each of them splitting into two. Ultimately, the population size remains constant. To simulate elimination–dispersal phenomenon, some bacteria are liquidated at random with a very small probability, while the new replacements are randomly initialized over the search space. At the end of search process, the bacteria reach at the global optimum position.

Iterative algorithm for Enhanced Bacterial foraging optimization

Step 1: Initialization. To begin with, all the parameters related to proposed algorithm are initialized. Each particle in the group is assigned with a random initial position $\theta(i)$, and an initial velocity (v) which is a random number in the interval $[-1, 1]$ with elements $n(i)$; $n = 1, 2, \dots, P$.

Step 2: Preliminary assessment of bacterial population.

- (a) For $i = 1, 2, \dots, S$, current fitness ($J_{current}^i$) of each bacterium in the search space is determined as per the following expression.

$$J_{current}^i = J(i, j, k, l)$$

- (b) In the beginning of search process, since the bacterial movement is not yet started, the local best fitness (J_{local}^i) and local best position (x_{lbest}^i) of each bacterium are its current fitness value and current position respectively, i.e.

$$J_{local}^i = J_{current}^i$$

$$x_{lbest}^i = \theta(i, j, k, l)$$

- (c) The initial global best fitness (J_{global}) of the population is the minimum value of fitness possessed by any of the particle in the population and can be given by,

$$J_{global} = \min(J_{local}^i)$$

where $i = 1, 2, \dots, S$.

The position corresponding to J_{global} is assigned the global best position (x_{Gbest}^i).

Step 3: Iterative algorithm.

- (a) Initially the counters for chemotactic loop (j), reproduction loop (k), elimination–dispersal loop (l), and counter for swim length (m) are all set to zero.
- (b) Taking into account the cell-to-cell attractant effect, the cost function estimated for each of the $i = 1, 2, \dots, S$ bacteria is calculated as,

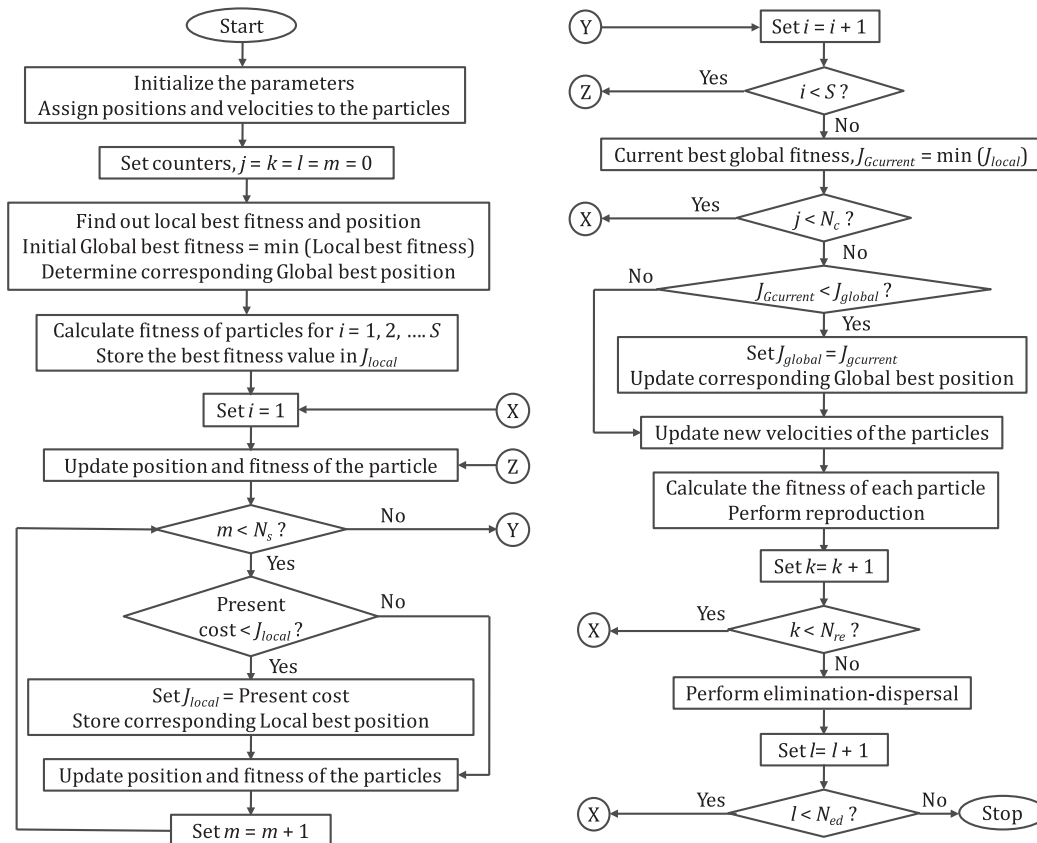


Fig. 4. Flowchart of Enhanced BFO algorithm.

$$J_{cc}(\theta(i, j, k, l)) = \sum_{i=1}^S \left[-d_{att} \cdot \exp \left(-w_{att} \sum_{n=1}^P (\theta_n - \theta_n^i)^2 \right) \right] \\ + \sum_{i=1}^S \left[h_{rep} \cdot \exp \left(-w_{rep} \sum_{n=1}^P (\theta_n - \theta_n^i)^2 \right) \right]$$

$$J(i, j, k, l) = J(i, j, k, l) + J_{cc}(\theta(i, j, k, l))$$

$$J_{last} = J(i, j, k, l)$$

The best cost function value is stored in J_{last} until a further better cost is obtained and the best cost of each bacterium (J_{local}^i) is updated as,

$$J_{local}(i, j, k, l) = J_{last}(i, j, k, l)$$

(c) Chemotactic loop: Starting with $i = 1$, the position and cost function for all the S number of bacteria in the entire population are updated using the expressions,

$$\theta(i, j + 1, k, l) = \theta(i, j, k, l) + C(i) \frac{v_k^i}{\sqrt{(v_k^i)^T \cdot v_k^i}}$$

$$J(i, j + 1, k, l) = J(i, j, k, l) + J_{cc}(\theta(i, j + 1, k, l))$$

While $m < N_s$,

If $J(i, j, k, l) < J_{local}$,

Then set $J_{local} = J(i, j, k, l)$.

Updating position and cost function we will get,

$$\theta(i, j + 1, k, l) = \theta(i, j, k, l) + C(i) \frac{v_k^i}{\sqrt{(v_k^i)^T \cdot v_k^i}}$$

$$J(i, j + 1, k, l) = J(i, j, k, l) + J_{cc}(\theta(i, j + 1, k, l))$$

The current position ($x_{current}$) of each bacterium can be given by,

$$x_{current}(i, j + 1, k, l) = \theta(i, j + 1, k, l)$$

The position corresponding to local best fitness (J_{local}^i) is stored in x_{Lbest}^i .

Increment the counter as, $m = m + 1$.

End the while loop.

To proceed to next bacterium, set $i = i + 1$ until $i = S$.

(d) In each chemotactic step, calculate the current global best fitness function value ($J_{Gcurrent}$) and continue the chemotactic loop if still $j < N_c$.

$$J_{Gcurrent} = \min(J_{local}^i)$$

where $i = 1, 2, \dots, S$.

If $J_{Gcurrent} < J_{global}$, set $J_{global} = J_{Gcurrent}$. The global best position (x_{Gbest}^i) is updated with the position corresponding to J_{global} .

(e) The particles update their new velocities and directions by the equation,

$$v_{k+1}^i = w \cdot v_k^i + c_1 \cdot r_1 [x_{Lbest}^i - x_{current}^i] + c_2 \cdot r_2 [x_{Gbest}^i - x_{current}^i]$$

(f) Reproduction:

The health of each bacterium is calculated using the expression given below and then sorted in ascending order of cost function.

$$J_{health}^i = \sum_{j=1}^{N_r+1} J^i(j, k, l)$$

S_r is the number of least healthy bacteria that are discarded out of the population and individuals with best health are split into two, keeping the population size constant.

(g) If $k < N_{re}$, continue with the next reproductive iteration by setting, $k = k + 1$.

The entire iterative process is executed repeatedly until the specified number of reproductive steps (generations) are executed.

(h) Elimination–dispersal loop:

With a probability of P_{ed} , the elimination–dispersal event is performed to ease the exploration of new search areas that may lead to better optimal solution.

If elimination–dispersal loop counter $l < N_{ed}$, execute successive elimination–dispersal events with the increment of counter l after each iteration.

Terminate the iterative process when the counter l reaches its maximum specified value, i.e., the number of elimination–dispersal events N_{ed} .

Problem formulation

Regulation of inverter dc-link voltage

The dc-side capacitor (C_{dc}) serves two major purposes, i.e. (i) maintains a constant dc voltage with small ripples in the steady state and (ii) serves as an energy storage element to supply real power difference between load and source during the transient period. The dc bus voltage must be higher than peak value of utility voltage, to force the output current of APF under the command of compensating current. This dc-link capacitor acts as an energy source and maintains energy balance inside the VSI. The component of supply reference current (i_{d1h}) to restore the energy on dc bus is computed based on energy balance. If V_{dc}^* is the reference value of dc-link voltage, nominal stored energy (e_{dc}^*) on the dc bus of APF is

$$e_{dc}^* = C_{dc} \frac{(V_{dc}^*)^2}{2} \quad (11)$$

The actual average stored energy (e_{dc}) on dc bus is given by (12), where V_{dca} is the average value of actual dc-link voltage.

$$e_{dc} = C_{dc} \frac{(V_{dca})^2}{2} \quad (12)$$

Thus energy loss (Δe_{dc}) of dc-link capacitor is

$$\Delta e_{dc} = e_{dc}^* - e_{dc} = C_{dc} \left\{ \frac{(V_{dc}^*)^2}{2} - \frac{(V_{dca})^2}{2} \right\} \quad (13)$$

This energy difference encountered in APF is supplied from ac mains by regulating the dc-link voltage with the help of a PI controller.

A PI controller offers dual advantages as the Proportional (P) action provides fast response and the Integral (I) action provides zero steady-state error. Block diagram for the process with PI controller is shown in Fig. 5.

The output of a PI controller is given by,

$$u(t) = K_p \cdot e(t) + K_i \int_0^t e(t) \cdot dt \\ = K_p \cdot [r(t) - c(t)] + K_i \int_0^t [r(t) - c(t)] \cdot dt \quad (14)$$

Here, t represents the instantaneous time, $e(t)$ is the system error between the desired output $r(t)$ and actual output $c(t)$, $u(t)$ is the controlled input for non-linear system, K_p is the proportional gain, and K_i is the integral gain. The proportional term considers only the current value of error at any time, whereas the integral term considers the sum of instantaneous errors over time, or how far the actual measured output value has been from the reference since

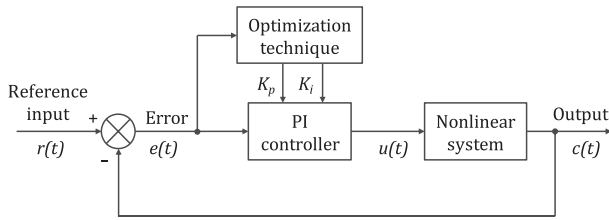


Fig. 5. Block diagram for PI controller design with optimization technique.

the start time. Here, the dc-link voltage error ($\Delta V_{dc} = V_{dc}^* - V_{dc}$) is minimized using a PI controller and the controller output is expressed in (15).

$$i_{d1h} = K_p \cdot \Delta V_{dc} + K_i \int_0^t \Delta V_{dc} \cdot dt \tag{15}$$

Need for optimization

In conventional linear PI controller tuning methods based on mathematical modeling, the recommended settings are empirical in nature and are obtained from extensive experimentation. Apart from this, the power system network presents itself as highly complex, non-linear and time varying system that involves large number of inequality constraints. Hence, to satisfy the conditions of both dynamics and stability, optimized values of gains K_p and K_i can always be obtained. The advantages of optimization based controllers over conventional controllers are: (i) no need of accurate mathematical modeling, (ii) can work with imprecise inputs, (iii) can handle nonlinearity, and (iv) more robust than conventional controllers.

Objective function and optimization parameters

Here, optimization parameters are the PI controller gains K_p and K_i in the range $0 < K_p < 100$ and $0 < K_i < 100$. Maximum overshoot, rise time, settling time and steady-state error are the constraints that imply optimality of a PI controller. Performance criterion chosen in this paper is integral square error (ISE) that treats both positive and negative errors equally. The objective function to be optimized (J_{ISE}) is formulated as per (16).

$$J_{ISE}(K_p, K_i) = \int_0^t (\Delta V_{dc})^2 dt \tag{16}$$

Simulation results

Extensive simulation has been carried out in MATLAB/Simulink and Opal-RT Lab in order to find out the effectiveness of APF with

Table 1
Values of system parameters used in simulation.

Parameter	Notation	Value
Supply frequency	f	50 Hz
Source impedance	(R_s, L_s)	(10 mΩ, 50 μH)
Load-1 parameters	$(R_{L1}, L_{L1}), (R_{dc1}, L_{dc1})$	(0.1 Ω, 3 mH), (25 Ω, 25 mH)
Load-2 parameters	$(R_{L2}, L_{L2}), (R_{dc2}, L_{dc2})$	(0.1 Ω, 3 mH), (25 Ω, 60 mH)
dc-link capacitance	C_{dc}	3 mF
Reference dc-link voltage	V_{dc}^*	800 V
ac-side filter parameters	(R_c, L_c)	(0.1 Ω, 1 mH)

Table 2
Values of parameters used in Optimization techniques.

Parameter	Notation	Value
Population size	S	8
Maximum no. of iterations	N	50
Dimension of search space	P	2
Acceleration constants	C_1, C_2	1.2, 0.12
Inertia constant	w_{max}, w_{min}	0.9, 0.4
No. of chemotactic steps	N_c	5
Length of swim	N_s	3
No. of reproduction steps	N_{re}	10
No. of elimination-dispersal steps	N_{ed}	3
Probability of elimination-dispersal events	P_{ed}	0.25
Coefficients of swarming for attractant signal	d_{att}, w_{att}	0.01, 0.04
Coefficients of swarming for repellent effect	h_{rep}, w_{rep}	0.01, 10

the above discussed optimization techniques under three different supply conditions. System configuration of shunt APF along with the three-phase non-linear diode rectifier loads is depicted in Fig. 6. Values of all the system parameters used for simulation and parameters used in optimization techniques are clearly indicated in Tables 1 and 2 respectively. For ideal supply, completely balanced and sinusoidal voltage of 230 V RMS is considered. A highly distorted supply condition is simulated by incorporating 30% of 3rd harmonic component into the supply voltage. For unbalanced supply, voltage in one of the phases is 200 V RMS, while in other two it is 230 V RMS.

MATLAB simulation results

The convergence characteristics of Fig. 7 shows that, Enhanced BFO reaches at minima in least number of generations compared to PSO and BFO under all kinds of supply voltage conditions. Initially, only Load-1 is put into operation until $t = 0.1$ s in order to evaluate the harmonic compensation capability of APF. Performance under

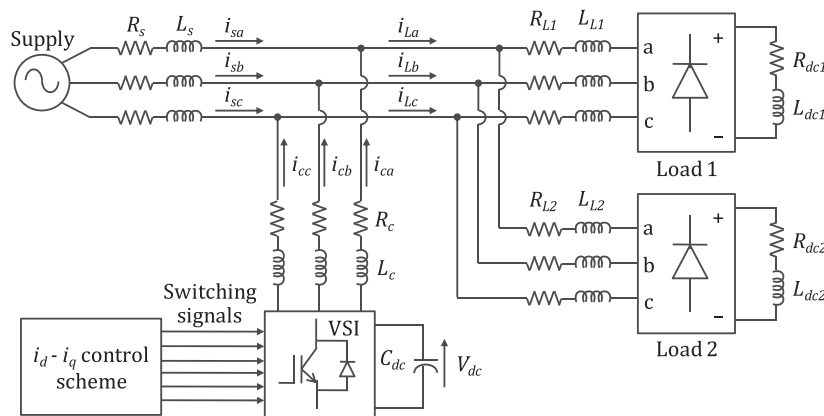


Fig. 6. VSI-based shunt APF system configuration along with the non-linear loads.

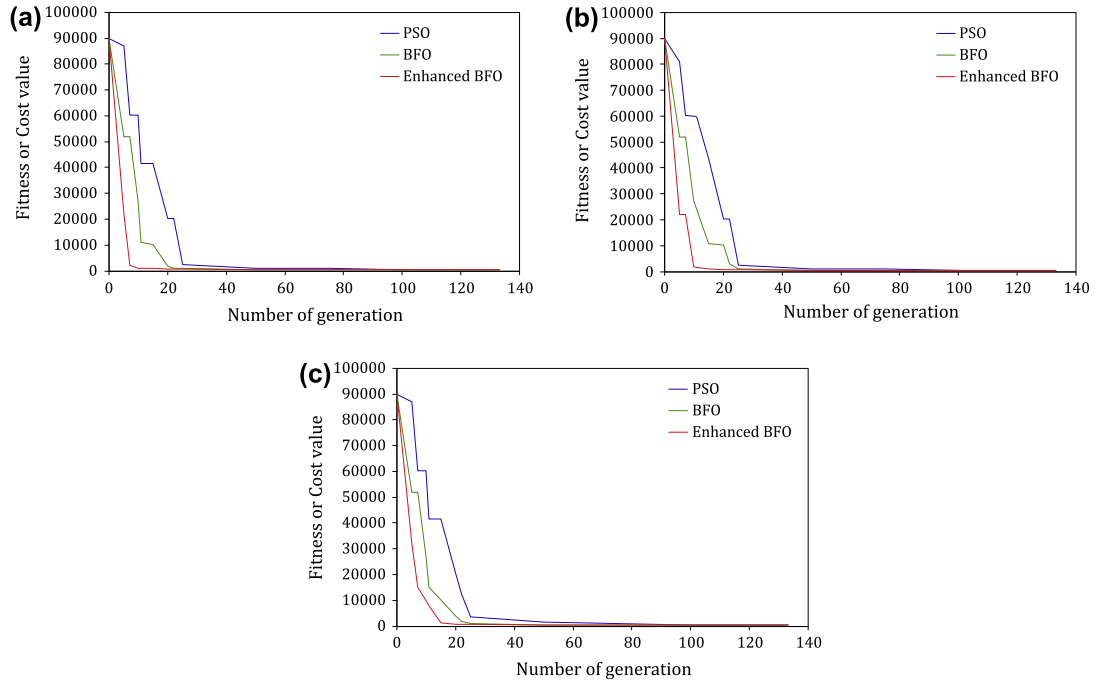


Fig. 7. Convergence characteristics of PSO, BFO and Enhanced BFO algorithms under (a) ideal supply, (b) distorted supply and (c) unbalanced supply.

dynamic conditions is observed by sudden switching on of Load-2 at time instant $t = 0.1$ s. Relative convergence of V_{dc} with Enhanced BFO, PSO and BFO based PI controllers has been shown in Fig. 8, which indicates that, V_{dc} reaches at its reference of 800 V within nearly one cycle under ideal and distorted supplies; and within 1.5 cycles under unbalanced supply. During load variation at $t = 0.1$ s, the deviation in V_{dc} is maximum for PSO and minimum for Enhanced BFO signifying its fast return to 800 V and hence quick prevail over harmonics. Besides, ripples in V_{dc} during steady state are observed to be very high for PSO and lowest for Enhanced BFO.

Figs. 9a–9c depict simulation waveforms for supply voltage, load current, compensation current, and source currents for APF employing PSO, BFO and Enhanced BFO under ideal, distorted and unbalanced supply conditions respectively. The nature of source current before compensation is exactly same as the load current. It can be clearly observed that, irrespective of the nature of supply condition, with the implementation of APF, harmonics in source current have been fully compensated by injecting suitable compensating filter currents. The nature of compensated source currents obtained with PSO, BFO and Enhanced BFO can be compared by Fast Fourier Transform (FFT) analysis. The THDs

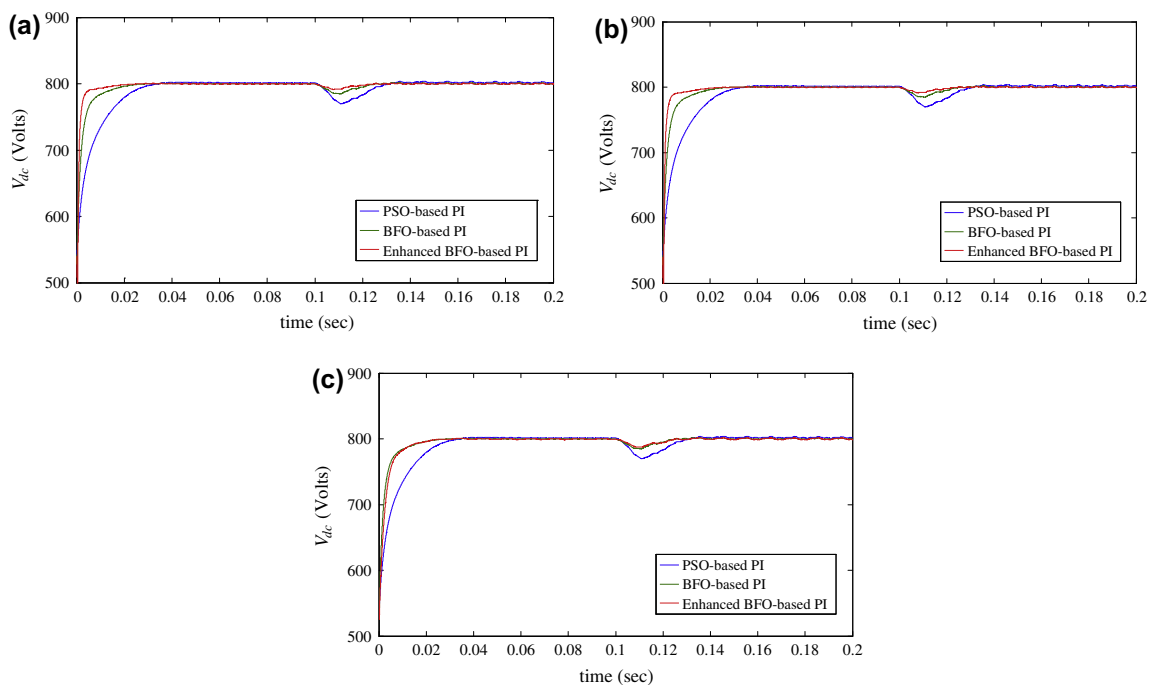


Fig. 8. Relative convergence of V_{dc} with PSO, BFO and Enhanced BFO-based APFs under (a) ideal supply, (b) distorted supply and (c) unbalanced supply.

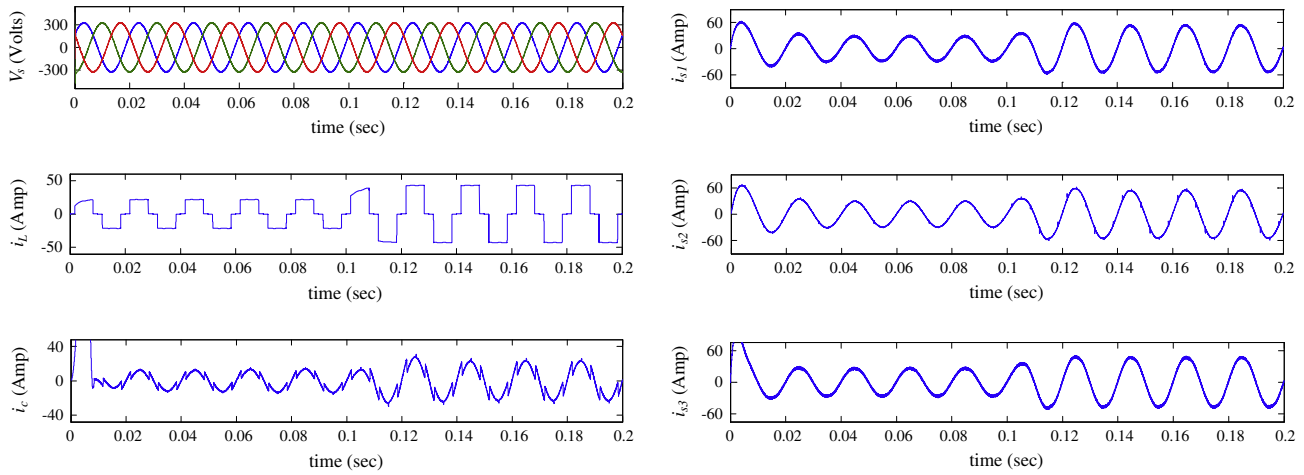


Fig. 9a. Simulation waveforms for supply voltage (V_s), load current (i_l), compensation current (i_c), and source currents for APF employing PSO (i_{s1}), BFO (i_{s2}) and Enhanced BFO (i_{s3}) under ideal supply.

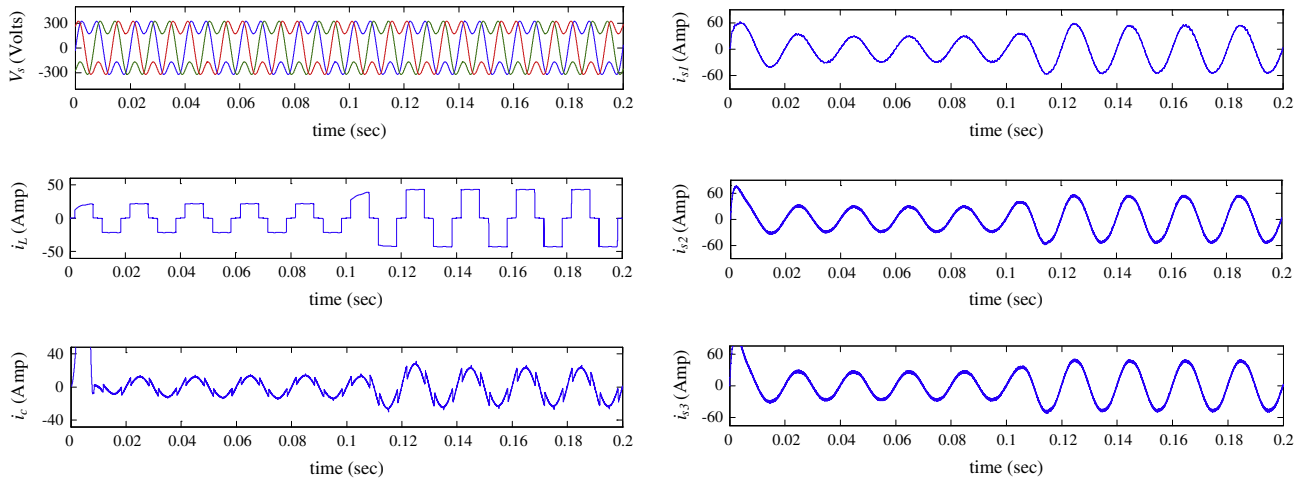


Fig. 9b. Simulation waveforms for supply voltage (V_s), load current (i_l), compensation current (i_c), and source currents for APF employing PSO (i_{s1}), BFO (i_{s2}) and Enhanced BFO (i_{s3}) under distorted supply.

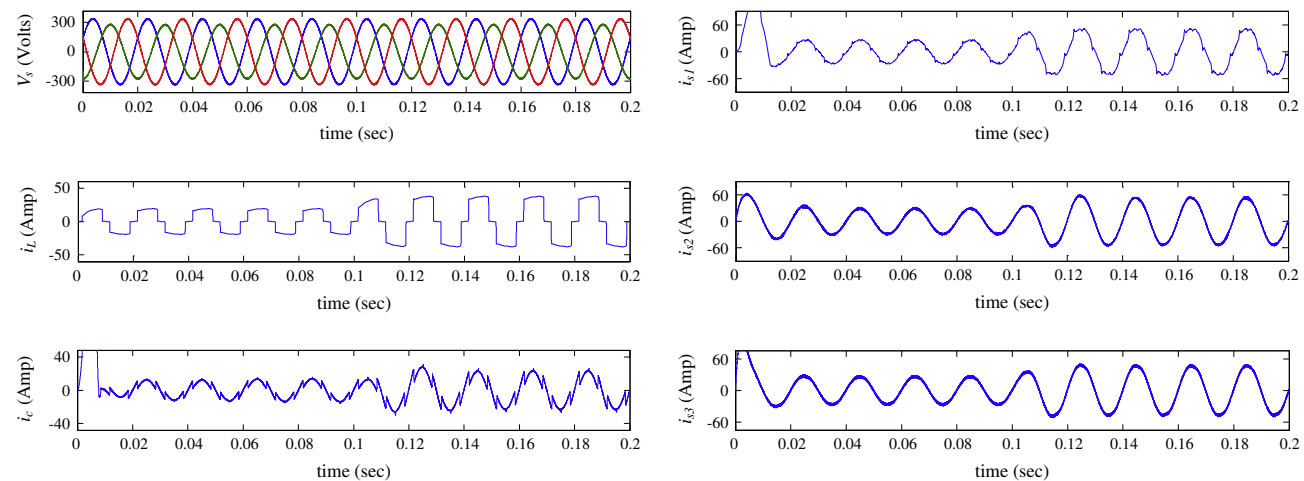


Fig. 9c. Simulation waveforms for supply voltage (V_s), load current (i_l), compensation current (i_c), and source currents for APF employing PSO (i_{s1}), BFO (i_{s2}) and Enhanced BFO (i_{s3}) under unbalanced supply.

obtained from this analysis have been tabulated in Table 3. The compensation of current harmonics to such a large extent irrespective of supply voltage is also due to the lower value of source impedance, which contributes to low influence of supply on source current and vice-versa.

Real-time performance analysis with Opal-RT Lab

The Simulink model is built in the PC installed with MATLAB, which is integrated with Opal-RT Lab simulator. Once the model is prepared, RT-Lab uses Real-Time Workshop to convert the separated models into code for compilation as subsystem simulations on each target processor. Data from the model is directed to the user via a special subsystem, called the Console, where the signals being generated can be viewed. In Fig. 10, the set-up used for real-time simulation via Opal-RT Lab is depicted and various components of OP5142 have been listed in Table 4. The details regarding each component are described in [15,43,44]. The PCI-Express port on OP5142 adapter board allows the users to connect the distributed processors together and operate at faster cycle times than ever before. This real-time link takes advantage of the FPGA power to deliver up to 2.5 Gbits/s full-duplex transfer rates. The OP5142 board is used to translate a Simulink design built using particular library blocks into HDL. The results are observed in a Digital storage oscilloscope (DSO).

Rigorous analysis of performances of APFs employing PSO, BFO and the proposed Enhanced BFO is done in RT-Lab by operating both the loads simultaneously and the results for ideal, distorted and unbalanced supply voltage conditions have been presented in Fig. 11. RT-Lab results can now be compared with corresponding MATLAB results. The waveforms for supply voltage, load current, compensation filter currents and compensated source currents waveforms are exactly similar in both MATLAB and RT-Lab simulations. THD values of source currents signify the major differences in their level of distortion. FFT analyses are done to find out the source current THDs under ideal, distorted and unbalanced supplies and are tabulated in Table 5. Comparative evaluation of

Table 3
Source current THDs obtained with MATLAB.

Supply condition	Source current THD (in %)			
	Without APF	PSO based APF	BFO based APF	Enhanced BFO based APF
Ideal	30.05	2.12	1.78	1.44
Distorted	30.77	2.27	1.89	1.32
Unbalanced	29.72	2.78	2.14	1.58

Table 4
Components of Opal-RT OP5142 board.

Sl. no.	Component name	Description
1	S1	FPGA engine manual reset
2	JTAG1	FPGA JTAG interface
3	JTAG2	CPLD JTAG interface
4	JUMP4	JTAG architecture selection
5	JTAG3	PCIe bridge JTAG interface
6	JTAG4	SerDes JTAG interface
7	JP1	PCIe & synchronization bus and power supply
8	J1/J2/J3	Backplane data, ID and I ² C interface
9	JUMP1	Identification EEPROM write protection
10	JUMP2	FPGA configuration mode selection
11	JUMP3	Flash memory write protection
12	J4	Flash memory forced programming voltage

FPGA – Field-Programmable Gate Array, JTAG – Joint Test Action Group, CPLD – Complex Programmable Logic Device, PCIe – Peripheral Component Interconnect Express, SerDes – Serializer/Deserializer, I²C – Inter-Integrated Circuit, EEPROM – Electrically Erasable Programmable Read-Only Memory

source current THDs reveal that, Enhanced BFO offers lesser THDs than PSO and BFO under ideal, distorted and unbalanced voltage supplies.

Technical specifications of OP5142 RT-Lab:

(i) Digital I/O:

Number of channels: 256 input/output configurable in 1- to 32-bit groups
Compatibility: 3.3 V
Power-on state: High impedance

(ii) Bus:

Dimensions (not including connectors): PCI-Express x1
Data transfer: 2.5 Gbit/s

(iii) FPGA:

Device: Xilinx Spartan 3
I/O Package: fg676
Embedded RAM available: 216 Kbytes
Clock: 100 MHz
Platform options: XC3S5000
Logic slices: 33,280
Equivalent logic cells: 74,880
Available I/O lines: 489

Technical specifications of the PC used for RT-Lab simulations:

Microsoft Windows XP (32-bit version), Xilinx ISE design suite v10.1 with IP update 3, Xilinx System Generator for DSP v10.1, MATLAB R2007b.

Technical specifications of the computer used for MATLAB simulations: Microsoft Windows 7 (32-bit version), MATLAB R2009a.

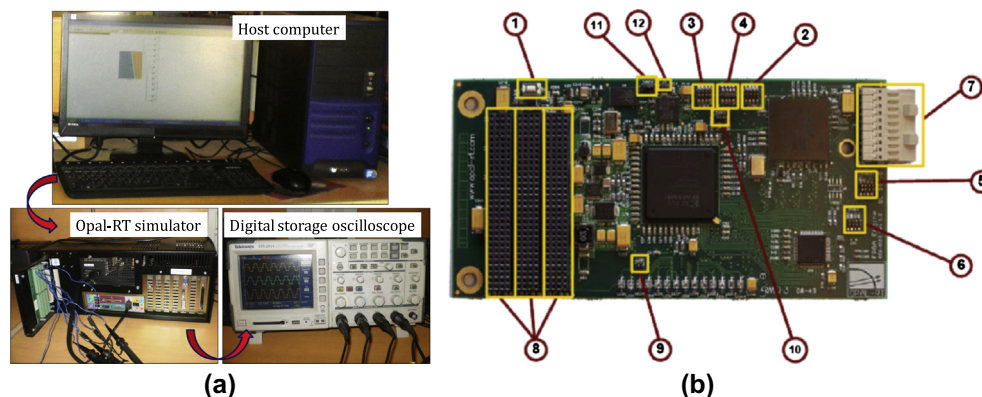


Fig. 10. Opal-RT Lab (a) set-up and (b) OP5142 system integration diagram showing layout and connectors.

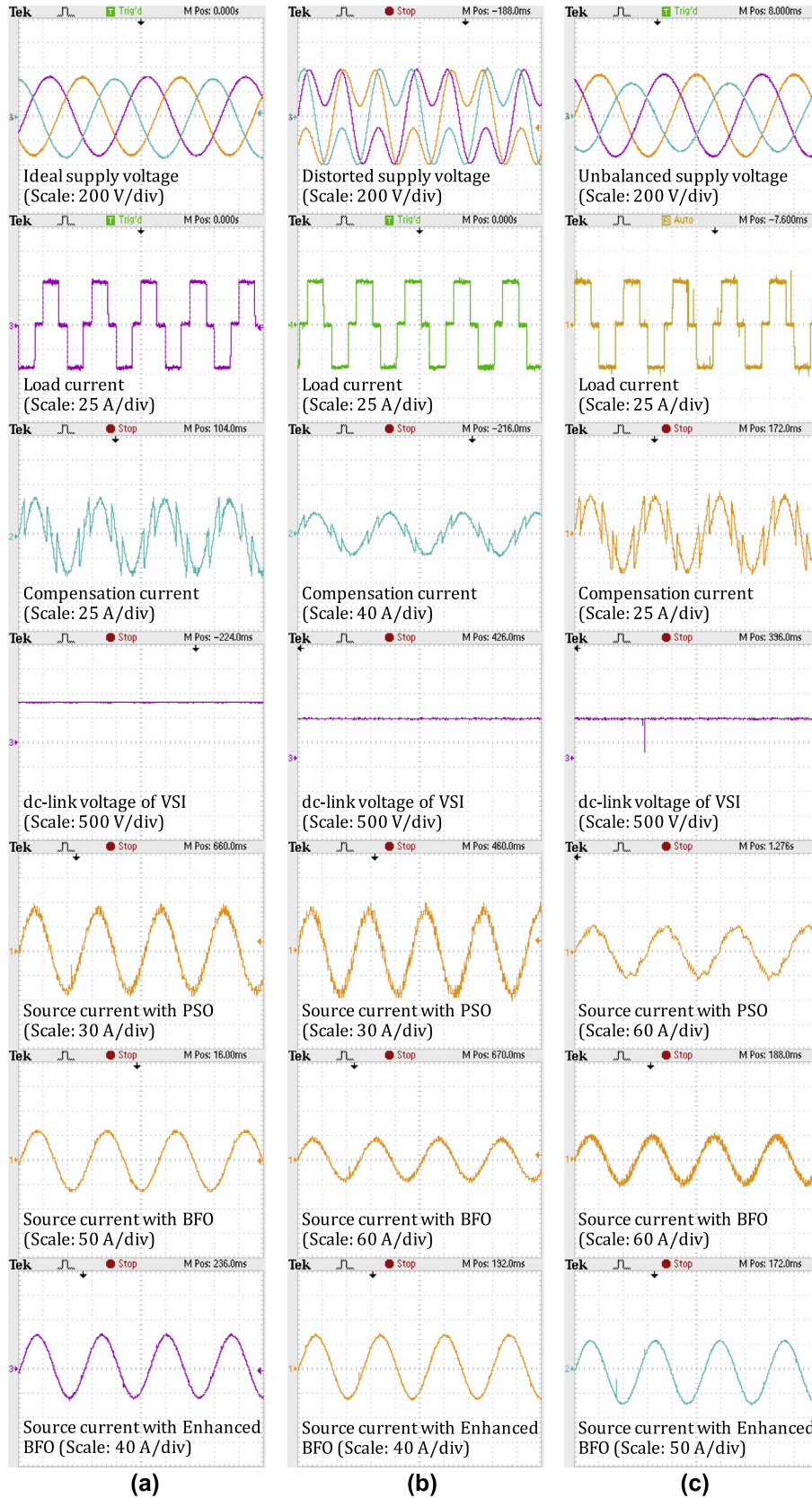


Fig. 11. RT-Lab results for supply voltage, load current, compensation filter current, dc-link voltage, source current for PSO-based APF, source current for BFO-based APF, source current for Enhanced BFO-based APF for (a) ideal supply, (b) distorted supply and (c) unbalanced supply respectively.

Table 5

Source current THDs obtained with Opal-RT Lab real-time simulator.

Supply condition	Source current THD (in %)			
	Without APF	PSO based APF	BFO based APF	Enhanced BFO based APF
Ideal	32.45	3.45	3.11	2.67
Distorted	33.30	3.59	3.22	2.62
Unbalanced	32.07	4.60	3.39	2.91

Conclusion

Our study proposed the development of a novel Enhanced BFO optimization strategy by hybridization of PSO and BFO to tune the proportional and integral gains of a PI controller. We proposed the implementation of this Enhanced BFO-based PI controller to be used for dc-link voltage regulation in APFs. Rigorous MATLAB and RT-Lab simulations are performed by employing PSO, BFO and Enhanced BFO algorithms to shunt APF, keeping the simulation parameters and system configuration same in all the cases. It showed that, Enhanced BFO technique gives excellent V_{dc} transient response as the deviation of dc-link voltage from its reference value could be minimized in the smallest amount of time (approximately one cycle) irrespective of the supply voltage and sudden load change conditions. Hence, it provides nearly instantaneous compensation over current harmonics. The natures of compensated source currents obtained with various optimization approaches are compared to find out the relative harmonic distortion in them. Less steady state ripples in V_{dc} transient leads to brilliant dc-link voltage regulation, resulting in less distorted source currents in case of Enhanced BFO. It outperformed all other alternatives in current harmonics mitigation by yielding the least values of source current THDs. Hence, Enhanced BFO algorithm has an edge over the classical BFO and PSO algorithms, especially in context to the convergence behavior of the algorithm very near to the desired solution. This fact has been supported here both analytically and experimentally using MATLAB and Opal-RT Lab.

References

- [1] Peng FZ. Harmonic sources and filtering approaches. *IEEE Ind Appl Mag* 2001(July/August):18–25.
- [2] Subjak JS, Mcquilkin JS. Harmonics – causes, effects, measurements, and analysis: an update. *IEEE Trans Ind Appl* 1990;26(6):1034–42.
- [3] IEEE recommended practices and requirements for harmonic control in electric power systems, 993, IEEE Standard 519-1992.
- [4] Blooming TM, Carnovale DJ. Harmonic convergence – IEEE Std. 519-1992 helps define application of harmonic limits. *IEEE Ind Appl Mag* 2007(January/February):21–7.
- [5] Singh B, Al-Haddad K, Chandra A. A new control approach to three-phase active power filter for harmonics and reactive power compensation. *IEEE Trans Power Syst* 1998;13(1):133–8.
- [6] Singh B, Al-Haddad K, Chandra A. A review of active filters for power quality improvement. *IEEE Trans Ind Electron* 1999;46(5):960–71.
- [7] Akagi H. New trends in active filters for power conditioning. *IEEE Trans Ind Appl* 1996;32(6):1312–22.
- [8] Fujita H, Akagi H. A practical approach to harmonic compensation in power systems – series connection of passive and active filters. *IEEE Trans Ind Appl* 1991;27(6):1020–5.
- [9] Wu CJ, Chiang JC, Yen SS, Liao CJ, Yang JS, Guo TY. Investigation and mitigation of harmonic amplification problems caused by single-tuned filters. *IEEE Trans Power Del* 1998;8:800–6.
- [10] Chiang SJ, Ai WJ, Lin FJ. Parallel operation of capacity limited three-phase four-wire active power filters. *Proc Inst Electr Eng Electr Power Appl* 2002;149(5):329–36.
- [11] Montero M, Cadaval ER, Gonzalez FB. Comparison of control strategies for shunt active power filters in three-phase four-wire systems. *IEEE Trans Power Electron* 2007;22(1):229–36.
- [12] Vardar K, Akpınar E, Surgevil T. Evaluation of reference current extraction methods for DSP implementation in active power filters. *Electr Power Syst Res* 2009;79(May):1342–52.
- [13] Bhattacharya A, Chakraborty C, Bhattacharya S. Shunt compensation: reviewing traditional methods of reference current generation. *IEEE Ind Electron Mag* 2009(September):38–49.
- [14] Soares V, Verdelho P, Marques GD. An instantaneous active and reactive current component method for active filters. *IEEE Trans Power Electron* 2000;15(4):660–9.
- [15] Patnaik SS, Panda AK. Real-time performance analysis and comparison of various control schemes for particle swarm optimization-based shunt active power filters. *Electr Power Energy Syst* 2013;52:185–97.
- [16] Jain SK, Agarwal P, Gupta HO. Design simulation and experimental investigations, on a shunt active power filter for harmonics, and reactive power compensation. *Electr Power Compon Syst* 2003;31(7):671–92.
- [17] Mishra S, Bhende CN. Bacteria foraging technique-based optimized active power filter for load compensation. *IEEE Trans Power Del* 2007;22(1):457–65.
- [18] Patnaik SS, Panda AK. Particle swarm optimization and bacterial foraging optimization techniques for optimal current harmonic mitigation by employing active power filter. *Appl Comput Intell Soft Comput* 2012;2012:1–10.
- [19] Chang W-D, Shih S-P. PID controller design of nonlinear systems using an improved particle swarm optimization approach. *Nonlinear Sci Numer Simul* 2010;15:3632–9.
- [20] Gaing Z-L. A particle swarm optimization approach for optimum design of PID controller in AVR system. *IEEE Trans Energy Conv* 2004;19(2):384–91.
- [21] Lin C-L, Jan H-Y, Shieh N-C. GA-based multiobjective PID control for a linear brushless dc motor. *IEEE/ASME Trans Mechatron* 2003;8(1):56–65.
- [22] Uyyuru KR, Mishra MK, Ghosh A. An optimization-based algorithm for shunt active filter under distorted supply voltages. *IEEE Trans Power Electron* 2009;24(5):1223–32.
- [23] Verma V, Singh B. Genetic-algorithm-based design of passive filters for offshore applications. *IEEE Trans Ind Appl* 2010;46(4):1295–303.
- [24] Kumar P, Mahajan A. Soft computing techniques for the control of an active power filter. *IEEE Trans Power Del* 2009;24(1):452–61.
- [25] Alrashidi MR, El-Hawary ME. A survey of particle swarm optimization applications in power system operations. *Electr Power Compon Syst* 2006;34(12):1349–57.
- [26] Abido MA. Optimal power flow using particle swarm optimization. *Electr Power Energy Syst* 2002;24:563–71.
- [27] Shayeghi H, Shayanfar HA, Jalilzadeh S, Safari A. A PSO based unified power flow controller for damping of power system oscillations. *Energy Convers Manage* 2009;50(10):2583–92.
- [28] He N, Xu D, Huang L. The application of particle swarm optimization to passive and hybrid active power filter design. *IEEE Trans Ind Electron* 2009;56(8):2841–51.
- [29] Chen M-R, Li X, Zhang X, Lu Y-Z. A novel particle swarm optimizer hybridized with extremal optimization. *Appl Soft Comput* 2010;10:367–73.
- [30] Monson CK, Seppi KD. Adaptive diversity in PSO. In: *Proc 8th annual conference on genetic and evolutionary computation*, ACM Press, New York; 2006. p. 59–66.
- [31] Passino KM. Biomimicry of Bacterial foraging for distributed optimization and control. *IEEE Control Syst Mag* 2002;22(June):52–67.
- [32] Mishra S. A hybrid least square-fuzzy bacterial foraging strategy for harmonic estimation. *IEEE Trans Evol Comput* 2005;9(February):61–73.
- [33] Das TK, Venayagamoorthy GK. Bio-inspired algorithms for the design of multiple optimal power system stabilizers: SPPSO and BFA. In: *IEEE industry application society's 41st annual meeting*, Tampa, USA, October 2006. p. 635–41.
- [34] Mishra S, Tripathy M, Nanda J. Multi-machine power system stabilizer design by rule based bacteria foraging. *Electr Power Syst Res* 2007;77:1595–607.
- [35] Tripathy M, Mishra S. Bacteria foraging-based solution to optimize both real power loss and voltage stability limit. *IEEE Trans Power Syst* 2007;22(1):240–8.
- [36] Kim DH, Abraham A, Cho JH. A hybrid genetic algorithm and bacterial foraging approach for global optimization. *Inf Sci* 2007;177(18):3918–37.
- [37] Biswas A, Dasgupta S, Das S, Abraham A. Synergy of PSO and bacterial foraging optimization: a comparative study on numerical benchmarks. In: *2nd International symp hybrid artificial intelligent systems, advances in soft computing series*, Springer Verlag, Germany, innovations in hybrid intelligent systems, ASC, vol. 44; 2007. p. 255–63.
- [38] Biswas A, Dasgupta S, Das S, Abraham A. A synergy of differential evolution and bacterial foraging optimization for faster global search. *Int J Neural Mass-Parallel Comput Inf Syst-Neural Netw World* 2007;8.
- [39] Azizpanah-Abarghoee R. A new hybrid bacterial foraging and simplified swarm optimization algorithm for practical optimal dynamic load dispatch. *Electr Power Energy Syst* 2013;49:414–29.
- [40] Tang WJ, Wu QH, Saunders JR. Bacterial foraging algorithm for dynamic environment. In: *IEEE congress on evolutionary computation*, Vancouver, Canada, July 2006. p. 4467–73.
- [41] Das S, Dasgupta S, Biswas A, Abraham A, Konar A. On stability of the chemotactic dynamics in bacterial foraging optimization algorithm. *IEEE Trans Syst Man Cyber – Pt A* 2009;39(3):670–9 [IEEE Press, USA].
- [42] Biswas A, Das S, Abraham A, Dasgupta S. Analysis of the reproduction operator in an artificial bacterial foraging system. *Appl Math Comput* 2010;215:3343–55.
- [43] RT-Lab Professional. <<http://www.opal-rt.com/product/rt-lab-professional>>.

- [44] Patnaik SS, Panda AK. Three-level H-bridge and three H-bridges-based three-phase four-wire shunt active power filter topologies for high voltage applications. *Electr Power Energy Syst* 2013;51:298–306.
- [45] Akagi H. Active harmonic filters. *Proc IEEE* 2005;93(12):2128–41.
- [46] Routimo M, Salo M, Tuusa H. Comparison of voltage-source and current-source shunt active power filters. *IEEE Trans Power Electron* 2007;22(2):636–43.
- [47] Kennedy J. The particle swarm: social adaptation of knowledge. In: *Proc 1997 international conference on evolutionary computation*, Indianapolis, IN, USA; 1997. p. 303–8.
- [48] Shi Y, Eberhart RC. A modified particle swarm optimizer. In: *Proc IEEE international conference on evolutionary computation*, Anchorage, AK, May 1998. p. 69–73.